Stem Cell Reports
Article
ISSCR
OPEN ACCESS

Inducing human retinal pigment epithelium-like cells from somatic tissue

Ivo Ngundu Woogeng,[1] Bogumil Kaczkowski,[2] Imad Abugessaisa,[2] Haiming Hu,[1] Akihiro Tachibana,[1] Yoshiki Sahara,[1,3,4] Chung-Chau Hon,[2] Akira Hasegawa,[2] Noriko Sakai,[1] Mitsuhiro Nishida,[1] Hashimita Sanyal,[1] Junki Sho,[1] Keisuke Kajita,[1] Takeya Kasukawa,[2] Minoru Takasato,[1,3] Piero Carninci,[2,5] Akiko Maeda,[1] Michiko Mandai,[1] Erik Arner,[2] Masayo Takahashi,[1] and Cody Kime[1,*]

[1]RIKEN Center for Biosystems Dynamics Research, Kobe 650-0047, Japan
[2]RIKEN Center for Integrative Medical Sciences, Yokohama 230-0045, Japan
[3]Laboratory of Molecular Cell Biology and Development, Department of Animal Development and Physiology, Graduate School of Biostudies, Kyoto University, Kyoto 606-8501, Japan
[4]Department of Renal and Cardiovascular Research, New Drug Research Division, Otsuka Pharmaceutical Co. Ltd., Tokushima 771-0192, Japan
[5]Human Technopole, Via Rita Levi Montalcini 1, Milan, Italy
*Correspondence: cody.kime@a.riken.jp
https://doi.org/10.1016/j.stemcr.2021.12.008

SUMMARY

Regenerative medicine relies on basic research outcomes that are only practical when cost effective. The human eyeball requires the retinal pigment epithelium (RPE) to interface the neural retina and the choroid at large. Millions of people suffer from age-related macular degeneration (AMD), a blinding multifactor genetic disease among RPE degradation pathologies. Recently, autologous pluripotent stem-cell-derived RPE cells were prohibitively expensive due to time; therefore, we developed a faster reprogramming system. We stably induced RPE-like cells (iRPE) from human fibroblasts (Fibs) by conditional overexpression of both broad plasticity and lineage-specific transcription factors (TFs). iRPE cells displayed critical RPE benchmarks and significant *in vivo* integration in transplanted retinas. Herein, we detail the iRPE system with comprehensive single-cell RNA sequencing (scRNA-seq) profiling to interpret and characterize its best cells. We anticipate that our system may enable robust retinal cell induction for basic research and affordable autologous human RPE tissue for regenerative cell therapy.

INTRODUCTION

The retinal pigment epithelium (RPE) is a monolayer of cuboidal cells developed between the photoreceptors and choroid of the eye. The RPE is critical for the development, maintenance, and function of photoreceptors, and mutations in key RPE genes such as *RPE65*, *BEST1/VMD2*, and *MERTK* may cause degenerative retinal disorders, Leber congenital amaurosis, Best macular dystrophy, and retinitis pigmentosa, respectively (Esumi et al., 2004; Gal et al., 2000; Gu et al., 1997; Petrukhin et al., 1998; Verbakel et al., 2018). Supplementation of RPE cells can recover from RPE dysfunction in animal models, suggesting a potential solution for retinitis pigmentosa (Haruta et al., 2004; Maeda et al., 2013). RPE degeneration onset is also associated with preceding age-related macular degeneration (AMD), the leading cause of irreversible blindness in western countries (Esumi et al., 2004; Klein et al., 1992; Smith et al., 2001). In AMD, RPE cells are damaged, and transplantation of healthy RPE cells may help hold disease progression (Mandai et al., 2017).

Recent advances in regenerative medicine have motivated new strategies to develop pluripotent stem-cell-derived RPE from human embryonic stem (ES) cells and autologous induced pluripotent stem cells (iPSCs) (Haruta et al., 2004; Mandai et al., 2017). RPE differentiation from pluripotent stem cells was pioneered against great technological and political barriers that were overcome with demonstrably safe and functional iPSC-derived RPE (iPSC.RPE) for patient transplant (Mandai et al., 2017). Still, uncertainties about iPSC potency and genome stability remain, and such novel regenerative medicine required labor and financing that are impossible to budget in modern health systems. Therefore, simplifying the induction of autologous RPE cells with a more direct approach may be necessary.

Lately, "direct reprogramming" systems that convert between somatic cell states (Najm et al., 2013; Pang et al., 2011; Zhang et al., 2014) have emerged, inspired by the transcription factor (TF) synergy famously uncovered by Kazu Takahashi and Shinya Yamanaka with iPSCs (Takahashi et al., 2007). Such systems posit that core TF sets should "directly" convert between somatic cell identities (D'Alessio et al., 2015; Rackham et al., 2016). Conceptually, "direct reprogramming" ignores epigenetic plasticity, or assumes it, with simplistic design for somatic-to-somatic cell state conversion and a focus on target cell state predominant TFs. In practice, such systems usually rely on Yamanaka-factor (*OCT4*, *SOX2*, *KLF4*, *MYC*) co-induction, or transit cell progenitor and intermediate plastic states yet bound by *time* and a *surviving identity*. Yet unlike somatic cell identities, induced pluripotency enables increasing plasticity via pioneering TF driven epigenetically self-recursive state reinforcement, termed "maturation," that was obviated

much later (Iwafuchi-Doi and Zaret, 2014; Samavarchi-Tehrani et al., 2010; Soufi et al., 2012; Soufi and Zaret, 2013). Even the roundly accepted "induced neuron" system was fortuitously built on the incredible pioneering TF *ASCL1*, whose mechanisms were understood later (Pang et al., 2011; Soufi et al., 2015). Once minimally established, truly reprogrammed genomes self-iterate and stabilize often at a multipotent or generative identity. Other fundamentally different approaches apply small molecules to reprogram or direct cell fates (Maruotti et al., 2015; Zhao et al., 2015).

To reduce autologous cell production time and induce RPE (iRPE) from fibroblasts (Fibs), we hypothesized that TFs with pioneering activity, direct roles in plasticity, and the developmental differentiation and specification of RPE may be required (Soufi et al., 2015). We found that four TFs (*MITF*, *OTX2*, *LIN28*, *MYCL*), enhanced by *CRX* and small molecules, could convert human Fibs to bulk cultures containing RPE-like cells with characteristic function, expression, cell identity, and integration in chimeric subretinal transplants. Together, our iRPE platform and single-cell RNA sequencing (scRNA-seq) datasets may help develop affordable autologous biomedical-grade regenerative RPE cell therapies.

RESULTS

Diverse exogenes may reprogram human somatic cells to RPE-like fate

Autologous iPSC.RPE for cell therapy (Mandai et al., 2017) has a multiplier for costs based on time. Seeking affordability, we set out to induce human somatic cells much more quickly to RPE cells (e.g., 200 days > 60 days) (Figure 1A). We looked to a previous "direct reprogramming" study (Zhang et al., 2014) whose TFs failed in our hands (data not shown). That system relied on *PAX6*, which was also required in a subsequent iRPE study that could not maintain RPE cell fate without sustained expression (D'Alessio et al., 2015).

Unlike previous reports, we found that a conditionally expressed *MITF*, *OTX2*, *LIN28*, *MYCL*, and *CRX* could rapidly induce human foreskin Fibs to RPE-like cells with tacit features of RPE summarized in Figure 1. These factors were selected for RPE cell-specific (*MITF*, *CRX*, *OTX2*), retina/neuroectoderm lineage-specific (*CRX*, *OTX2*), and pluripotency/plasticity/regenerative roles (*OTX2*, *LIN28*, *MYCL*). To do so, we employed lentiviral transduction to introduce a molecular toolset containing a common minimized *BEST1* (*VMD2*) (Esumi et al., 2004; Masuda and Esumi, 2010; Zhang et al., 2014) synthetic reporter construct to drive EGFP expression (*BEST1::*EGFP) and a constitutive polycistronic sequence with dox-inducible rTTA and puromycin resistance (PuroR) (Figure 1B). Fibs were transduced with the toolset, selected briefly with Puromycin, expanded, and then transduced with dox-inducible TetRE transgenes (Figure S1A). Importantly, the *BEST1::*EGFP reporter responded to iPSC.RPE cell maturity and density with similar expression in our RPE-like cells. We sub-cultured picked colonies of such iRPE-like cells and validated RPE65 protein expression among the EGFP+ cells (Figure 1C). We termed these induced RPE-like cells "iRPE."

Individually sub-cultured iRPE colonies did not proliferate or expand much past 0.64 cm^2 (Figure S1B); therefore, we bulk-passaged our full 6 W well 1:2 on approximately days 28–30 (Figure 1D). With this system, we generally observed distinct morphological change and mesenchymal to epithelial transition (MET) between days 5 and 10 and specific cobblestone RPE-like morphology with variable activation of *BEST1::*EGFP between days 12 and 25 and variable stability after removal of doxycycline (Figure 1D). Importantly, we could generate high numbers of cells resembling RPE with important markers such as RPE65, LHX2, TYRP1, and ZO-1 in tight junctions with gross similarity to model RPE cells (Figures 1C and S1C). Taken together, these observations reinforced the notion that our iRPE system may transition through important MET-mediated cell identity reprogramming with genome stability selectivity (Kareta et al., 2015; Li et al., 2010; Marión et al., 2009; Samavarchi-Tehrani et al., 2010) and then acquire important features and reporters of RPE cell identity (Maruotti et al., 2015; Masuda and Esumi, 2010; Zhang et al., 2014).

Orthodenticle genes are powerful effectors of iRPE reprogramming

Previous reports had resolved or hypothesized (Rackham et al., 2016) iRPE system factors (Figure 2A), but did not turn off reprogramming factor expression (Zhang et al., 2014) or observed a return to Fib identity when doing so (D'Alessio et al., 2015). Both reports that demonstrated iRPE cell output utilized Orthodenticle homeobox 2 (*OTX2*), a powerful gene expressed from the arrangement and induction of primed pluripotency through development to the eye, and then the RPE (Buecker et al., 2014; Esumi et al., 2009; Hever et al., 2006; Thomson and Yu, 2012).

A well-known retinal development TF, Orthodenticle homeobox 3, is commonly called Cone-Rod homeobox protein (*CRX*) (Esumi et al., 2009). In early tests, we isolated iRPE colonies for expansion and performed genomic DNA PCR for our reprogramming transgenes and found that transgenic *MITF* was not common, yet the Orthodenticle homeobox TFs *CRX* and *OTX2* were detected in all clones (Figure S1D). We found that excluding *CRX* resulted

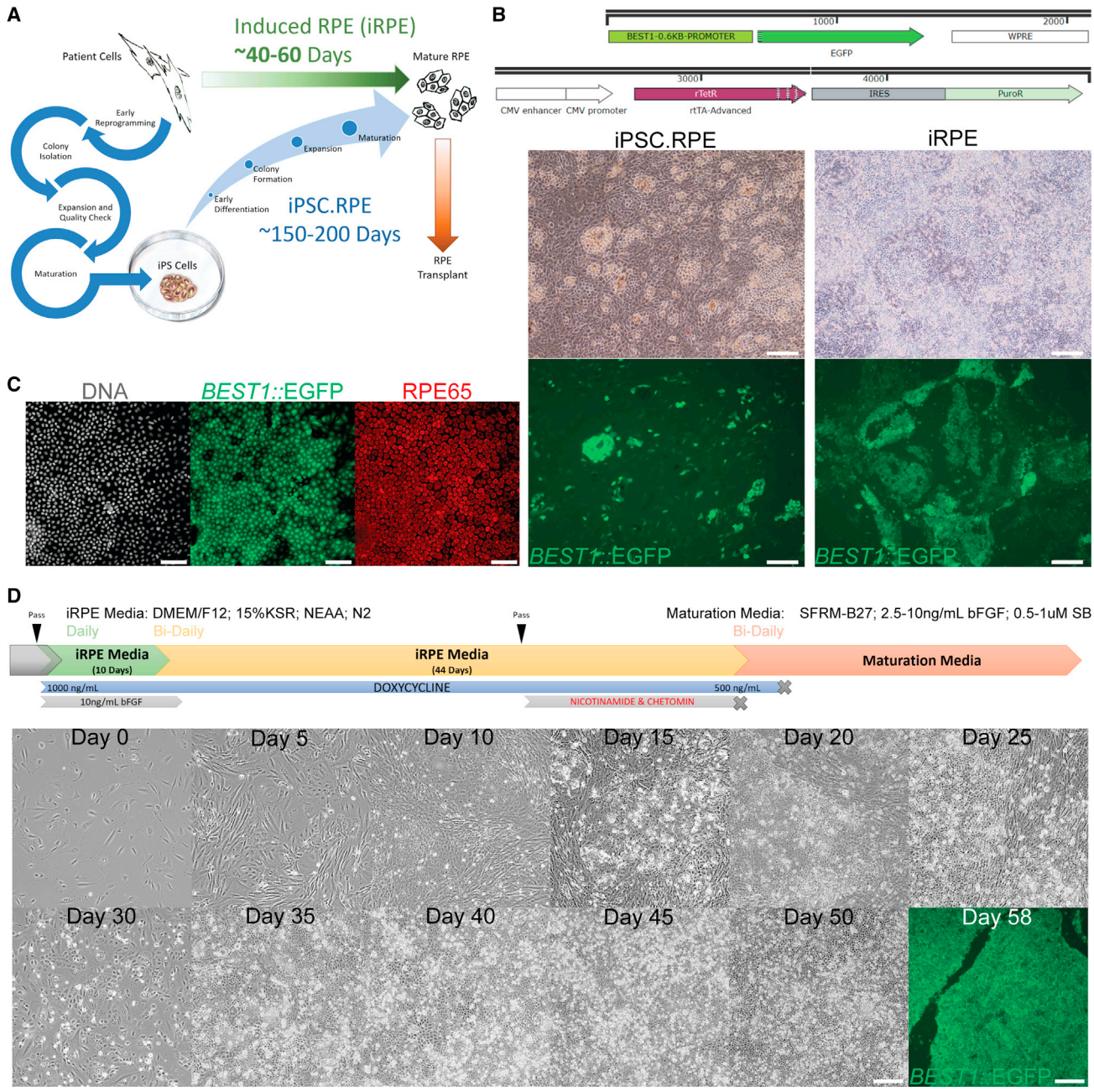

Figure 1. iRPE system overview

(A) A iRPE system objectives schematic and estimated time frames compared with autologous iPSC.RPE.

(B) *BEST1*::EGFP synthetic promoter reporter construct and constitutive (CMV)-driven conditional dox-inducible system (rTetR/rtTA) with PuroR. Construct is integrated and expressed in iPSC.RPE (left) and iRPE (right). Scale bars = 200 μm.

(C) Sub-cultured iRPE colony expressing *BEST1*::EGFP with immunocytochemistry for DNA (white; Hoechst 33,342) and RPE65 (red). Scale bar = 100 μm.

(D) A schematic (upper) and pictorial (lower) representation of iRPE reprogramming with basal media compositions and supplementations, timing of molecules and conditional reprogramming (doxycycline). Scale bars = 100 μm.

in significant reductions in iRPE colony counts and diameters (Figure 2B). We therefore retained *CRX* and *OTX2* in our core iRPE system experiments.

Among all previous iRPE reports (Figure 2A) and other "direct reprogramming" systems, the pioneering TF *PAX6* (Soufi et al., 2015) was common, and we anticipated that

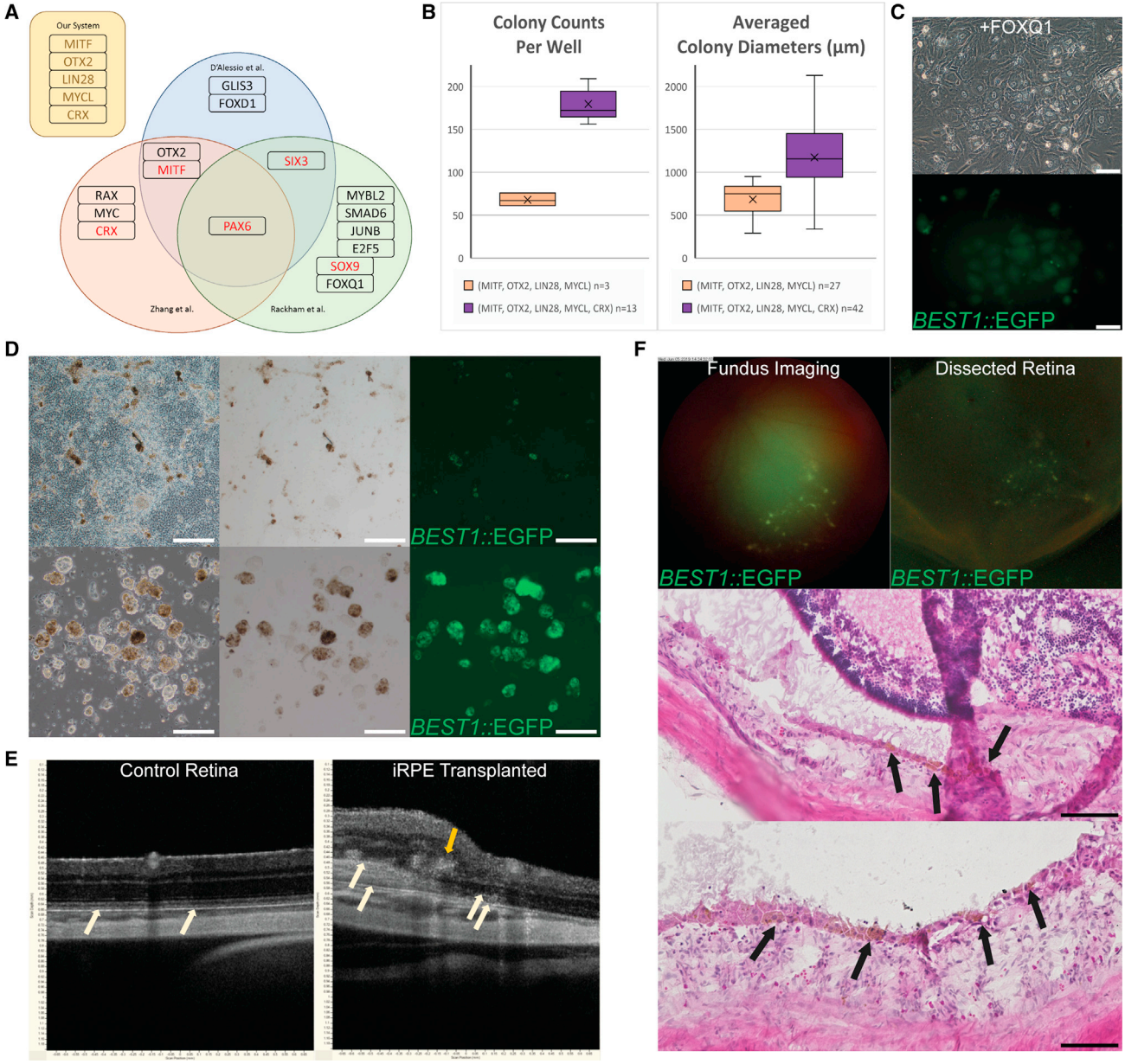

Figure 2. iRPE systems, TF testing, and preliminary subretinal transplantation

(A) A Venn diagram of the TFs from our iRPE system and each previous iRPE study (D'Alessio et al., 2015; Rackham et al., 2016; Zhang et al., 2014).

(B) iRPE reprogramming +/− CRX, with colonies counted per independent 6 W on day 9 (left) and average independent colony diameters measured on day 13 (right). Mean markers (x) and outliers are labeled. Colony number two-sample t test one-tail p value = 6.75953×10^{-8}. Colony diameter two-sample t test one-tail p value = 3.66273E-10.

(C) Day 9 iRPE system + FOXQ1 colony expressing *BEST1::*EGFP. Scale bars = 100 μm.

(D) Pre (upper) and post (lower) iRPE cluster purification culture images to show morphology, pigmentation, and *BEST1::*EGFP expression. Upper scale bars = 500 μm, lower scale bars = 200 μm.

(E) OCT scans of untreated (left) and iRPE transplanted (right) albino rat retinas. Host and transplanted RPE/RPE-like layers are indicated (white arrows) with potential retinal transplant rosette formations (yellow arrow).

(F) Fluorescent imaging for *BEST1::*EGFP in live fundus (upper left) later dissected (upper right) iRPE transplanted retina, and that retina's cryosections with H&E staining (lower) to reveal pigmented human iRPE cells (black arrows) in RPE layers and subretinal space interfacing with host photoreceptor outer segments. Scale bars = 100 μm.

adding *PAX6* would improve our system. We added dox-inducible *PAX6* to our reprogramming set (*MITF*, *OTX2*, *LIN28*, *MYCL*, *CRX*) and observed a broad change in cell morphology by day 3, followed by a striking cell death event and total ablation of all colony forming cells by day 6, leaving no visible colonies for an extended period thereafter (data not shown). Alternative iRPE reprogramming factors *FOXQ1* and *SOX9* were also added to our system. However, both factors caused premature activation of the *BEST1::*EGFP reporter, rendering its RPE maturation/identity-reporting features useless (Figure 2C). Furthermore, *FOXQ1*+ reprogramming induced small EGFP+ colonies with little to no visible proliferation by day 9 (Figure 2C). For these reasons, we did not continue to use exogenous *PAX6*, *FOXQ1*, or *SOX9*.

Transplanted iRPE cells integrate and pigment in albino rat retinas

In preliminary tests, *BEST1::*EGFP+ iRPE cells were collected in floating pigmenting balls for purification similar to our previous iPSC.RPE production method (Kuroda et al., 2012). We pooled several floating pigmenting iRPE clusters to a well and sub-cultured for brief expansion (Figure 2D). We prepared immune-compromised albino rats with subretinal transplantation of iRPE cells. Within 2–3 months, we used optical coherence tomography (OCT) scans and usually found several affected areas with possible bulks of cells between the host RPE and photoreceptors. Notably, some cells in the bulked areas had structural and light characteristics that resembled the RPE layers. We also saw signs of xenografted cells in the photoreceptor layer, implicating rosettes often seen in RPE xenograft experiments (Figures 2E and S2A).

We observed EGFP+ cells during fluorescent live fundus imaging and dissection of the retinas (Figure 2F). Cryosections with hematoxylin and eosin (H&E) staining showed many pigmented cells had cobblestone morphology and were interfaced with photoreceptor outer segments and sometimes fully integrated into the RPE layer at various positions proximal to the injection site (Figure 2F).

Nicotinamide and Chetomin improves iRPE cell reprogramming

Previous reports showed that Nicotinamide (NIC) and Chetomin (CTM) treatments may improve pluripotent stem-cell-derived RPEs, such as iPSC.RPE (Maruotti et al., 2015; Williams et al., 2012). We bulk-passed iRPE cells to two wells and treated one well + CTM mid-reprogramming with the timing shown in Figure 1D. iRPE + CTM appeared to reduce *BEST1::*EGFP maturation reporter expression and cell pigmentation among significant cell debris/death, while the surviving cobblestone cell layer became morphologically more homogeneous than control cells (Figure 3A). Functional analysis using transwell cultures of human primary RPE (hRPE), iRPE, and iRPE + CTM had determined apical and basal PEDF and VEGF concentrations by ELISA, along with TER measurements, across a 4-week period (Figure S3A). Generally, iRPE and iRPE + CTM secreted PEDF and VEGF with apical/basal trends like the hRPE, although weaker. TER measurements were present but showed a lower initial TER with a 4-week increase when compared with hRPE. Interestingly, iRPE + CTM samples were improved over iRPE alone (Figure S3A). To test phagocytic function, we employed a popular FITC-labeled rod outer segment (FITC-ROS) phagocytosis assay (Iwasaki et al., 2016) with iPSC.RPE, iRPE that had NIC&CTM treatment, and Fib. Subsets of densely packed and *BEST1::*EGFP+ iRPE cells had mostly phagocytosed FITC-ROS similar to the iPSC.RPE; we validated the FITC-ROS with a specific antibody (Figure S3B).

To examine the effects of NIC and CTM to the iRPE system, we performed a larger bulk passage of cells to several wells and treated with NIC, CTM, or NIC&CTM (Figure S3C). Interestingly, NIC alone increased *BEST1::*EGFP expression over the control samples during treatment, and afterward, such cells increased pigmentation and bulging/blebbing in maturation. CTM alone followed the previously observed trend, decreasing *BEST1::*EGFP expression during treatment and mildly reduced cell pigmentation as cells matured. The combination of NIC&CTM again had notably increased cell death (Figure S3D) seen by CTM alone (Figure 3A) and, excitingly, had gained the benefits of each individual treatment with no notable negative effects. We therefore termed iRPE treated with NIC&CTM as "iRPENC" and added treatment to our standard method (Figure 1D).

During RPE purification, individually plated pigmented clusters can reveal a subjective basic quality based on outgrowth morphology, as shown with iPSC.RPE (Kuroda et al., 2012). We performed parallel experiments of iRPE and iRPENC originating from the same bulk passage taken to maturation and doxycycline removal. Purified pigmented floating clusters were plated to individual wells and outgrowths were assessed as "good" or "bad". We observed that iRPENC cultures produced many more "good" outgrowths (Figure 3B).

The interesting cell death from CTM treatments in iRPE reprogramming was not described in the previous iPSC.RPE differentiation study using CTM (Maruotti et al., 2015). Indeed, iRPE reprogramming is uniquely from Fib, and bulk passage retains some non-iRPE cells. We tested NIC&CTM treatments in early iRPE reprogramming and found that Fib and early iRPE colony formation were drastically reduced among cell death (Figure 3C). Interestingly, if treatment started on or after day 8, most colonies could survive the treatment among dying Fibs, indicating a

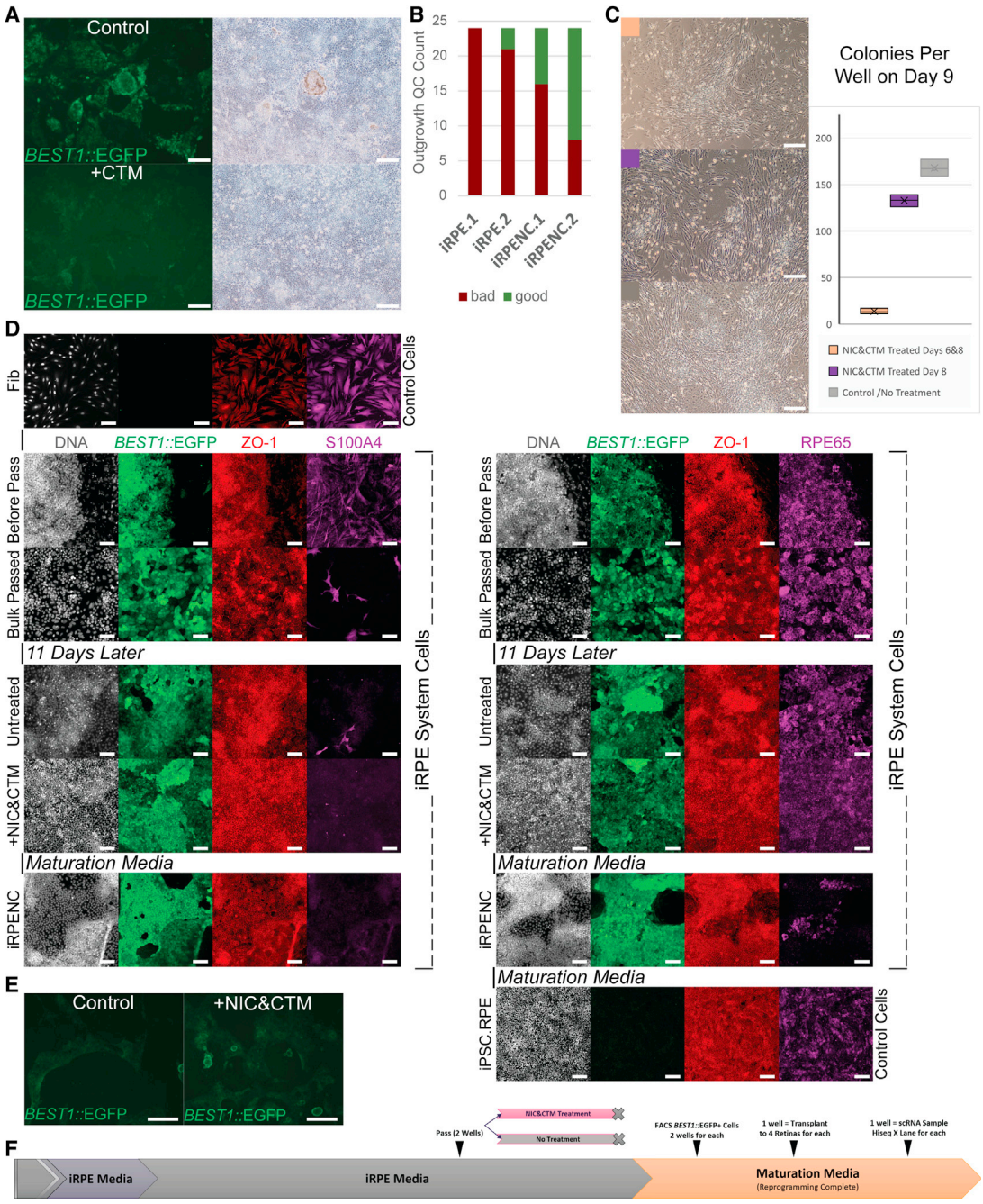

Figure 3. iRPE reprogramming cells treated with NIC and CTM

(A) A split iRPE culture +/− CTM treatment, during treatment, with *BEST1::*EGFP expression (left) and brightfield imaging (right). Scale bars = 200 μm.

(B) Subjective qualification (bad/good) of 24 individually plated iRPE cluster outgrowths from 2 iRPE and 2 iRPENC cultures.

(C) Effects of NIC&CTM treatments on early iRPE reprogramming cultures shown with brightfield microscopy (left) and independent iRPE 6 W colony counts on day 9 (right). Scale bars = 200 μm. Single-factor ANOVA p value = 3.08471×10^{-7}.

(D) Left: immunocytochemistry of Fib and iRPE system for DNA (white) *BEST1::*EGFP, (green) ZO-1 (red), and S100A4 (magenta). Right: immunocytochemistry of iRPE system and iPSC.RPE for DNA (white), *BEST1::*EGFP (green), ZO-1 (red), and RPE65 (magenta). Scale bars = 100 μm.

(legend continued on next page)

meaningful shift in reprogramming cell identity permissive to the small-molecule treatment (Figure 3C). Although early NIC&CTM treatment may prove useful, for the rest of this study, the timing was performed as in Figures 1D and 3F.

We wondered if NIC&CTM may be selective in our standard iRPENC method from Fib to RPE maturation and used immunocytochemistry for cell common ZO-1, Fib-specific marker S100A4, RPE-specific marker RPE65, and our *BEST1::*EGFP (Figure 3D). ZO-1 was weak but detectable on Fib surfaces and neatly lined tight junctions in likely iRPE and iPSC.RPE cell junctions. S100A4 labeled Fib, and before bulk passage a distinct layer of S100A4+ Fib underlay the *BEST1::*EGFP+ RPE65+ iRPE colonies that had neat ZO-1 junctions (Figure 3D). Bulk passage left few S100A4+ Fib cells, the iRPENC completely removed S100A4+ cells, and the increased cell death debris appeared to represent far more than suggested Fib numbers (Figure S3D). As usual, iRPENC morphology and stains homogenized with more consistent ZO-1+ cell-cell junctions and RPE65 than untreated iRPE. Interestingly, in maturation media, iRPENC cells diverged morphologically and subsets were variably *BEST1::*EGFP+ and RPE65+ (Figure 3D), a pattern that was replicated in another human dermal Fib line of iRPENC that were all LHX2+ with TYRP1+ subsets (Figure S3E). Taken together, the defined reprogramming media and bulk passage helped reprogramming iRPE outcompete non-reprogrammed Fib, the NIC&CTM treatment removed remaining Fib among iRPE homogenization and increased cell death, and then subsets of iRPENC variably retained RPE65 and TYRP1 expression during maturation (Figure 3D).

Coordinated *in vivo* retinal transplant and scRNA-seq experiments

Given the transplanted iRPE (Figures 2D–2F) and NIC&CTM treatments (Figures 3 and S3) data, we coordinated a transplant and scRNA-seq experiment with consistency from split parallel culture. We bulk-passed iRPE cells, cultured them with or without NIC&CTM treatment (iRPE/iRPENC), and then purified matured *BEST1::*EGFP+ cells by flow cytometry into two parallel 24 W wells (Figures 3E and 3F). After brief expansion, the cultures showed variable RPE-like stability. iRPENC cells maintained higher *BEST1::*EGFP expression among a greater area of cells and had more lasting RPE-like "bleb" that are common in high-quality iPSC.RPE cultures when cell junctions are tight and apical-basal flow bulges the RPE from the plate (Figures 3E and S3F; Videos S1 and S2) Unfortunately, several *BEST1::*EGFP+ iRPENC "blebs" had puckered and released from the plate and were lost during media changes. Ultimately, for each sample, parallel wells were sourced for subretinal transplantation and scRNA-seq analysis (Figure 3F).

Quality control with SkewC improves scRNA-seq sample distinction

For data consistency, we prepared iRPE, iRPENC, and control cell (Fib and iPSC.RPE) scRNA-seq libraries at the same time, read them at the same time, and then applied a quality control (QC) and read detection primary analysis workflow to prepare for various secondary analysis tools (Figure 4A). To QC our samples, we applied commonplace QC filtering (Luecken and Theis, 2019) and a new filtering method based on skewness of gene body coverage called SkewC (Abugessaisa et al., 2020), tested in parallel (Workflow 1; Figure S4A) and in series (Workflow 2; Figures 4B and S4A). Cells were labeled "Pass" or "Fail" based on commonplace QC filtering and "Typical" or "Skewed" based on SkewC. Both filters mostly labeled the same low-quality cells that clustered together yet SkewC frequently detected "Skewed" cells in cell clusters (Figures S4A and S4B) that had a "Pass" from commonplace QC. When we compared the Workflow 2 feature average expression level for RPE marker genes, variable features, and all detected features, the "Skewed" cells had higher average expression than "Typical" cells or no detection at all (Figure S4C). We interpreted that SkewC detected poor single-cell libraries that over-represented highly expressed reads and lacked lowly expressed reads. While both workflows improved analysis, Workflow 2 increased "Skewed" cell detection in desired clusters (Figure S4A) and was used for primary analysis QC (Figures 4A and 4B).

iRPENC is notably improved and has "high-quality" cells approaching subjective RPE identity

We used Seurat to perform uniform manifold approximation and projection (UMAP) analysis (Butler et al., 2018; McInnes et al., 2018; Stuart et al., 2019), which clustered Fib, iPSC, and iRPE/iRPENC samples separately (Figure 4C). Interestingly, we observed a distinct population between the iPSC.RPE and iRPE/iRPENC clusters predominately from iRPENC cells, suggesting that NIC&CTM treatment meaningfully improved iRPENC cells with lasting effect (Figure 4C). We compared iRPE to iRPENC and found that a distinct iRPENC subpopulation was the most enriched for *BEST1::*EGFP counts and important RPE features (*CRX, TYR, MERTK, LHX2*) (Figure 4D).

(E) A split iRPE culture that had previous +/− NIC&CTM treatments, prior to retinal transplant, expressing *BEST1::*EGFP among variable quality cells visible by brightfield (right). Scale bars = 500 μm.

(F) Overview of parallel subculture preparation for iRPE and iRPENC sample scRNA-seq analysis and albino rat subretinal transplant.

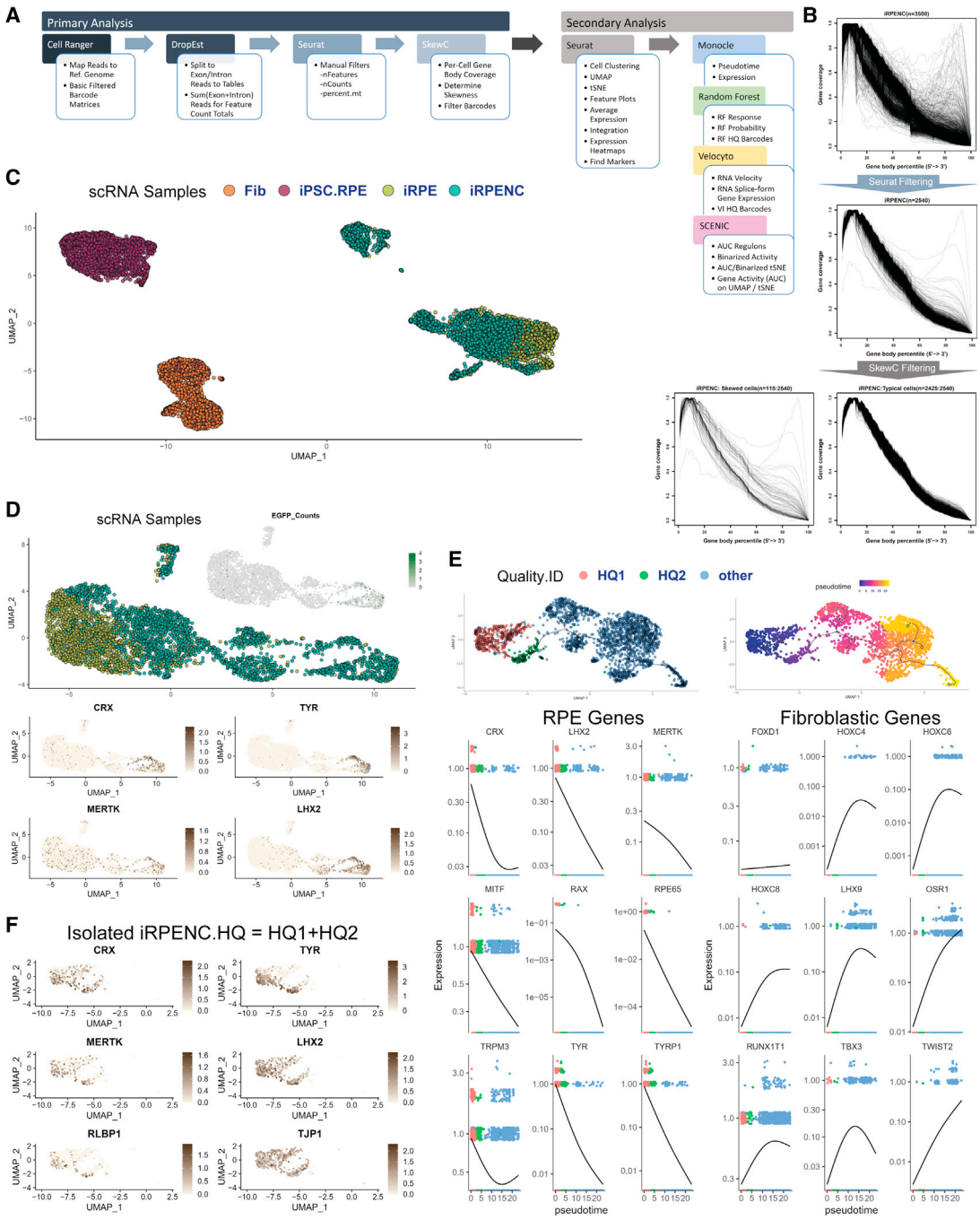

Figure 4. iRPE system scRNA-seq data preparation and preliminary analysis

(A) Overview of the primary and secondary analysis of scRNA-seq samples.

(B) Workflow 2 (serial) SkewC analysis total gene body mapped read traces, per cell after cell ranger (upper), after commonplace QC filtering in Seurat (mid), and then separated to skewed cell traces (lower left) and typical cell traces (lower right).

(C) Seurat UMAP plot of Fib, iRPE, iRPENC, and iPSC.RPE samples.

(D) Seurat UMAP plot of iRPE and iRPENC samples with coordinated inset plot of *BEST1::*EGFP counts (upper) and RPE feature plots (lower).

(E) Seurat UMAP coordinates of iRPENC plotted in monocle for HQ1, HQ2, and other, with pseudotime originating at the point of highest RPE gene and *BEST1:*EGFP expression (Figure S4D). Expression of RPE genes (left) and fibroblastic genes (right) are plotted across pseudotime and labeled with HQ1, HQ2, and other.

(F) Seurat UMAP-based RPE feature plots of iRPENC.HQ (HQ1 + HQ2).

We focused on iRPENC alone, and clusters 1 and 4 had the most *BEST1::*EGFP and RPE features (Figure S4D). We labeled the cells HQ1 (cluster 1), HQ2 (cluster 4), or "other." Pseudotime analysis (Trapnell et al., 2014) suggested that the "other" cells originated from the HQ1/HQ2 cell identities (Figure 4E). Across pseudotime, the HQ1 and HQ2 cells tended to be high in RPE genes and low in fibroblastic genes (Tomaru et al., 2014), while "other" cells showed the opposite (Figure 4E). Interestingly, the HQ1 and HQ2 fraction of cells predominately expressed *SERPINF1* (PEDF) and *VEGFA* (VEGF) (Figure S4E) that might explain why those secreted proteins were lower than control RPE cells in the functional tests (Figure S3A).

We thereafter combined HQ1 and HQ2 as "iRPENC.HQ" and labeled the remaining cells "iRPENC.other." Surprisingly, separating iRPENC.HQ and iRPENC.other neatly showed that iRPENC.HQ had mitochondrial gene fractions "percent.mt" matching iPSC.RPE, while iRPENC.other had not (Figure S4F). Expectedly, iRPENC.HQ broadly retained important RPE gene expression (Figure 4F), while iRPENC.-other did not (Figure S4G). Apparently, the iRPENC culture diverged leaving a stable "HQ" RPE-like population and a variably destabilized "other" population expressing some donor cell (Fib) TFs. The iRPENC.HQ were 531 of the total 2,425 iRPENC cells, representing 21.9% of the sample.

iRPENC and HQ subset may approach objective RPE identity

We sought to identify iRPENC cells objectively and used both random forest (RF) machine learning and RNA velocity to do so (Breiman, 2001; La Manno et al., 2018).

For RF, we imported the public 5k human peripheral blood mononuclear cell (PBMC) dataset to increase the size and diversity of the RF and labeled the 10 PBMC Seurat clusters (PBMC-CL0 to 9) (Figure 5A). The increased cell diversity clustered iRPENC much closer to iPSC.RPE (Figure 5A) and Fib cells farther away. We trained the RF on the PBMC, Fib, and iPSC.RPE samples and then tested the iRPENC.HQ and iRPENC.other samples against that RF. RF response determines a single identity and labeled most iRPENC cells with iPSC.RPE identity (Figure 5A, right). RF probability was more informative, showing high iPSC.RPE probability from iRPENC.HQ, where Fib probability was often zero, and mediocre iPSC.RPE probability in iRPENC.-other, where Fib probability was more frequent (Figure 5A, lower).

Since DropEst (Petukhov et al., 2018) (Figure 4A) parsed exon and intron counts, we examined RNA velocity with Velocyto (La Manno et al., 2018) on Seurat UMAP from our samples integrated on reference model iPSC.RPE (Figure 5B). Integration clustered iRPENC cells much closer to the reference than without, and RNA velocity showed that most clusters generally had arrows pointing inward, implicating stable states. Interestingly, a subset of iRPENC.HQ had RNA velocity toward iPSC.RPE, implicating ongoing change toward the iPSC.RPE state (Figure 5B). We labeled those cells "RNA Velocity Implicated," and they included 51 of the highest RF iPSC.RPE probability iRPENC cells (iPSC.RPE.prob >75%, Fib.prob <10%) (Figure 5B). Taken together with recurring cell clustering trends, we concluded that unique machine learning and bioinformatics tools could find agreement and identify high RPE likeness among dynamic and specific criteria in our unique system.

We further observed from the unspliced (u) and spliced (s) Velocyto plots of important RPE genes, that some RPE RNAs (*CDH1, FRZB, LHX2, TJP1*) were expressed typically in iRPENC.HQ as in iPSC.RPE, while other RPE genes (*RLBP1, TRPM1, TYR*) showed splice variance that related important epigenetic regulation was involved, and that the "RNA Velocity Implicated" cells were perhaps the most like iPSC.RPE (Figure 4B).

Integrating on iPSC.RPE as reference brought iRPENC and its iRPENC.HQ closer to iPSC.RPE in UMAP space, yet most cells overlapped in principal component space (Figure S5A), highlighting the importance of deeper analyses. We sought to improve analyses with external RPE data from a recently published ES cell-derived RPE study (Lidgerwood et al., 2020) that we labeled "ES.RPE.Young" and integrated with iPSC.RPE reference. ES.RPE.Young intermixed clustering with iPSC.RPE, and our iRPE system trend of reprogramming from Fib toward RPE became more apparent (Figure 5C). While positions across UMAP_2 appeared dynamic, positions across UMAP_1 reflected the spectrum across Fib and RPE identities. Those differences were not obvious by principal component analysis, where the ES.RPE.Young, iPSC.RPE, and iRPENC.HQ shared the same area, while Fib and iRPENC.other were further away (Figure S5B). A heatmap of gene expression based on specific molecular signatures of primary RPE cells and clinical iPSC.RPE cells (Kamao et al., 2014; Liao et al., 2010) showed that ES.RPE.Young, iPSC.RPE, and iRPENC.HQ shared a similar pattern, while Fib and iRPENC.-other also had a different shared pattern (Figure 5C, lower), which supported prior analyses (Figure 4E). To confirm that point, we checked expression for RPE markers (*CRX, TYR, RLBP1, RPE65, BEST1, RAX*) and found relatively comparable expression between the RPE models and iRPENC.HQ (Figure 5D).

Gene regulatory network analysis reveals distinct cell signatures

To better understand the reprogrammed state of iRPENC cells, we employed SCENIC (Aibar et al., 2017) to determine the gene regulatory network "regulons" learned from putative downstream expression at the single-cell

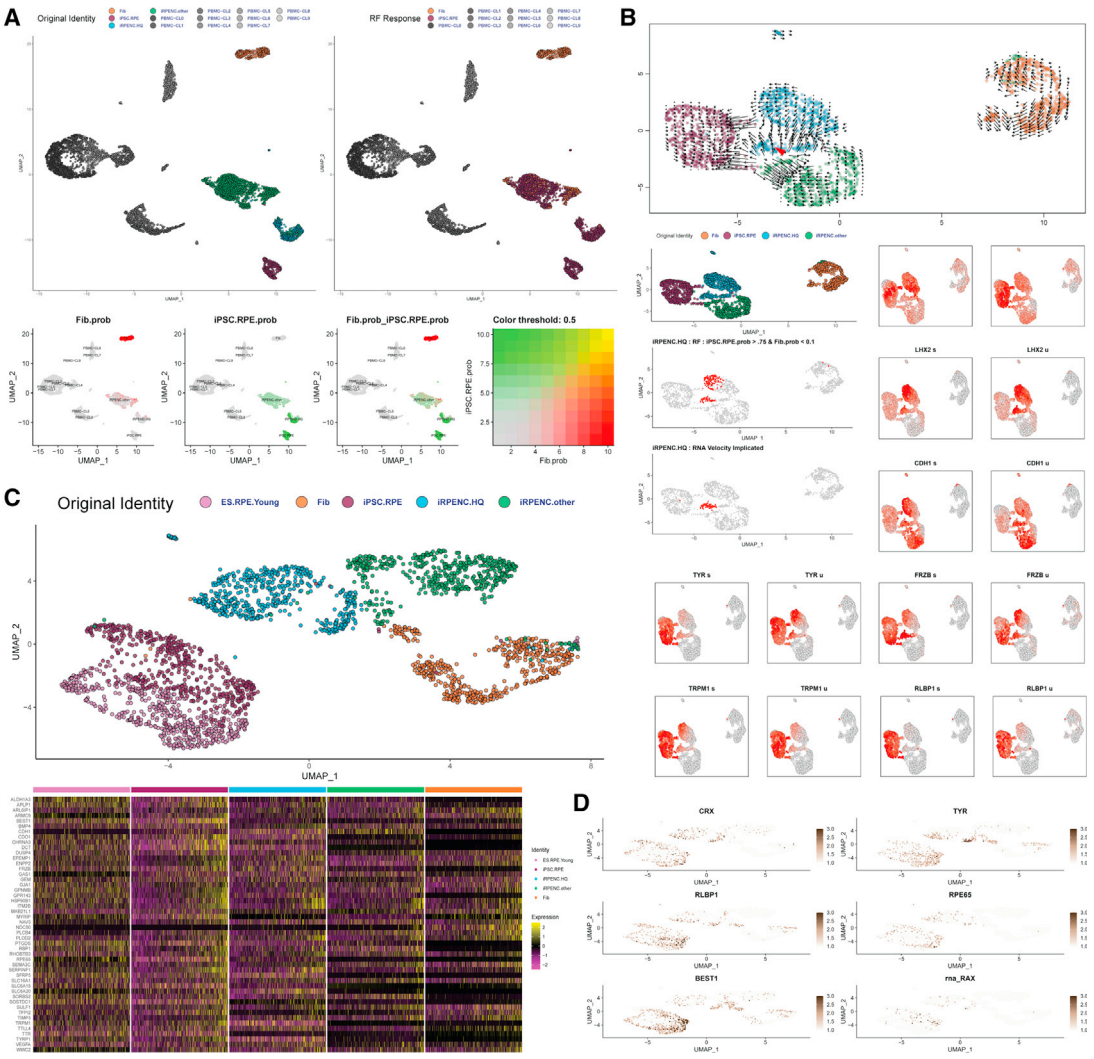

Figure 5. Machine learning and bioinformatics interpretation of iRPENC.HQ RPE identity

(A) Seurat UMAP plots of RF analysis samples labeled by original identity (upper left), RF response (upper right), and by Fib/iPSC.RPE probability (lower).

(B) Seurat UMAP plots with cell velocity (upper), identity (mid), and RF/RNA Velocity Implicated RPE-like iRPENC.HQ cells indicated in the cell velocity map (orange arrow) and highlighted in red (mid). RPE gene RNA detection by spliced/exon (s) and unspliced/intron (u) reads.

(C) Seurat UMAP plot of samples with reference-based integration on iPSC.RPE cells (upper), including RPE gene heatmap (lower).

(D) Seurat UMAP plot of (C) with RPE features CRX, TYR, RLBP1, RPE65, BEST1, and RAX.

level (Figure S6A). We compared Fib, iPSC.RPE, iRPENC.HQ, and iRPENC.other at equal cell numbers per sample and performed t-distributed stochastic neighbor embedding (tSNE) in Seurat (Figure S6B). Global regulon area under curve (AUC) by SCENIC/AUCell indicated iRPENC.HQ resembled iPSC.RPE with few differences (Figure S6C).

Many TFs operate in OFF/ON states relative to dosage and cofactor availability. In SCENIC analysis, thresholding regulon AUC histograms for binarization (OFF/ON) provided data that were easier to interpret (Figure 6A) than without binarization (Figure S6D). In all cases, the iPSC.RPE clustered with iRPENC and more closely to iRPENC.HQ (Figures 6A and S6D). A distinct set of Fib regulons was OFF in the iPSC.RPE and iRPENC.HQ samples (Figures 6A and S6A). Among the top 281 regulons, the pattern of iPSC.RPE and iRPENC.HQ regulon activity was similar in the higher and lower activity regulons (Figure 6A). Focusing on the strongest data and the cell reprogramming, we reduced to the top 55 regulons affecting >95% of cells in the analysis (Figure 6A), most Fib regulons were OFF in iRPENC.HQ, where most iPSC.RPE regulons were ON. Not surprisingly,

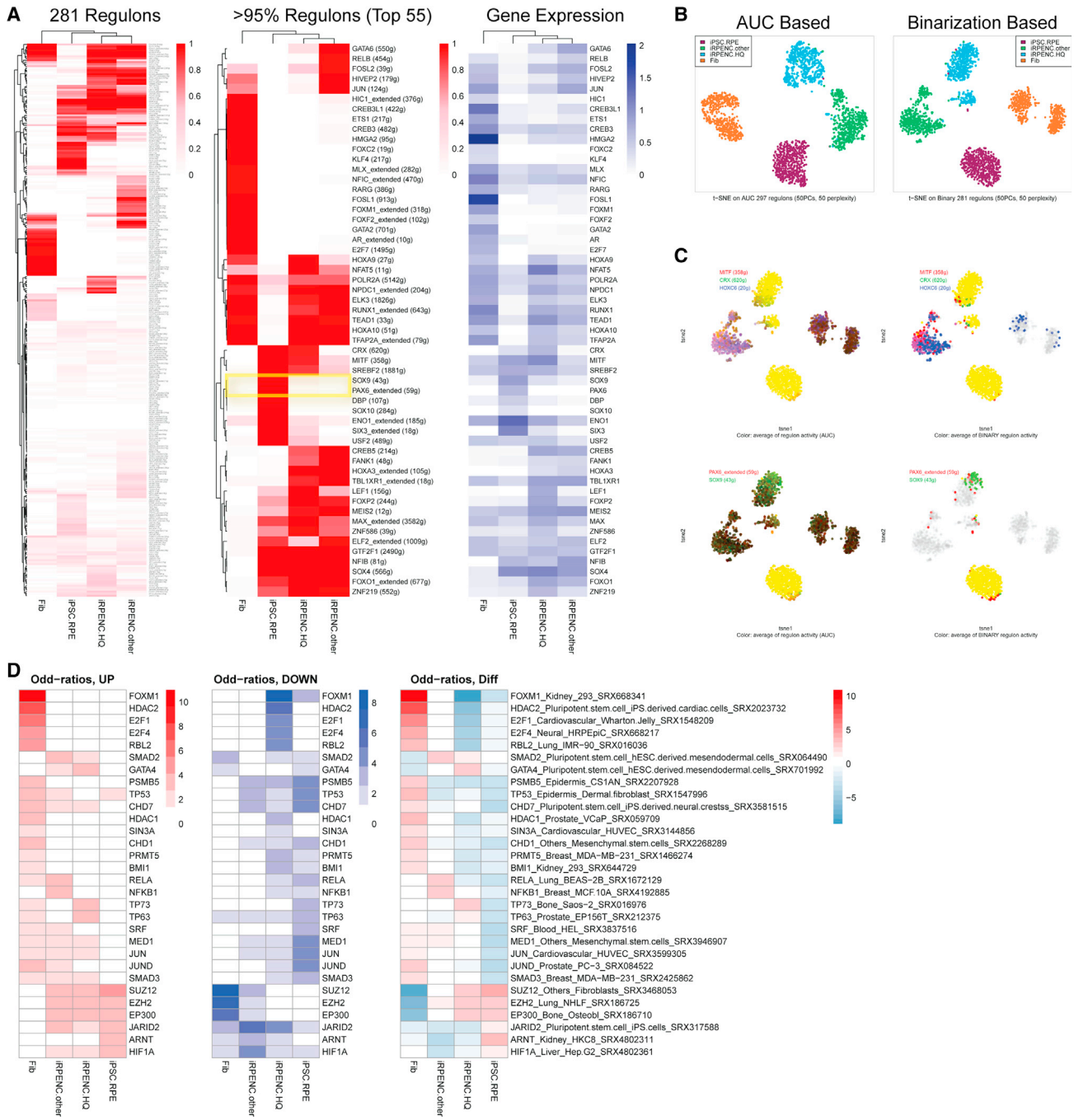

Figure 6. iRPE system genetic regulatory analysis

(A) SCENIC binarized regulons total (281, left), top 55 (mid) with heatmap (pheatmap) clustering and regulon activity (red scale), with row-matched TF expression (log-transformed TF gene expression averages per sample) (right). Yellow box highlights the SOX9 and PAX6_extended regulons.

(B) SCENIC AUC-based (left) and binarization-based (right) tSNE clusters of samples.

(C) AUC (left) and binarized (right) activity of MITF, CRX, HOXC6, PAX6_extended, and SOX9 regulons.

(D) Heatmap (pheatmap) of average gene expression signature enrichment for odd ratios UP (left, red scale), odd ratios DOWN (mid, blue scale), and combined with full ChIP-seq signature sample labeling (right).

both iRPENC groups had unique regulons that likely prevent closer clustering to model RPEs and inspire investigation. Of interest, the MITF and CRX regulons were strong in iRPENC.HQ, as in iPSC.RPE, showing that removing conditional reprogramming left their endogenous regulatory networks intact (Figure 6A). However, the SOX9 and PAX6_extended regulons were poor in iRPENC.HQ, restating their potential utility. Expectedly, averaged scRNA-seq counts for the TFs of the SCENIC-determined regulons provided a clear pattern relating TF expression and putative regulatory network downstream activity (Figure 6A).

We performed UMAP and tSNE analysis from regulon AUC and binarization (Figures 6B and S6E). UMAP provided distinct clustering (Figure S6E), and as reported with SCENIC (Aibar et al., 2017), the AUC- and binarization-based tSNE plots improved clustering over tSNE based on gene expression (Figures 6B and S6B). Curiously, in these plots and others in this report, a few iPSC.RPE clustered among the iRPENC.HQ.

To visualize individual cells, we selected the binarization-based tSNE plot to coordinate AUC and binarized regulon activity of MITF, CRX, and HOXC6 regulons. Expectedly, iRPENC.HQ and iPSC.RPE showed similar RPE regulons (MITF, CRX), while iRPENC.other and Fib showed the HOXC6 fibroblastic regulon (Figure 6C). Binarization thresholding can vary; for example, we set the CRX threshold to the highest of three normal distributions of AUC activity, where the iRPENC.HQ and iPSC.RPE were comparable, while the middle distribution was iRPENC.other and the lowest was Fib (Figure S6F). We also looked at candidate iRPE factor regulons PAX6_extended and SOX9 (Figures 6C and 2A), which showed a few iRPENC cells had strong PAX6_extended regulon, and a cluster of iRPENC.HQ had near full SOX9 regulon. We plotted the individual AUC plots for HOXC6, CRX, MITF, PAX6_extended, and SOX9 regulons across the UMAP and tSNE coordinates to clarify local enrichment (Figure S6G). Importantly, the "RNA Velocity Implicated" iRPENC.HQ cells agreed with the binarization-based tSNE and were the subset of cells closer to iPSC.RPE (Figures S6H and 5B). Taken together, completely unique SCENIC and Velocyto analyses could similarly implicate ideal RPE-like cells.

Next, we performed a customized analysis to understand which TFs may be responsible for the differences in groups. For each group, we generated a "signature" of UP and DOWN regulated genes (see experimental procedures). For each signature, we calculated Fisher's exact test enrichment of the overlap with ~10,000 experimentally derived chromatin immunoprecipitation sequencing (ChIP-seq) signatures from the ChIP Atlas (https://chip-atlas.org/; see experimental procedures). We selected the top 30 TF signatures with the highest variance of the odd ratios across the four groups (Figure 6D), avoiding redundancy by showing the most enriched ChIP-seq per unique TF.

For the upregulated signatures, the odd ratios of iRPENC.HQ showed a similar trend to iPSC.RPE and one different from Fib (Figure 6D). Many hits were broad regulatory TFs, and iPSC.RPE specifically had more enrichment for HIFs HIF1A and ARNT(HIF1B) (Figure 6D), raising curiosity about our HIF inhibitor CTM. Interestingly, iRPENC and iPSC.RPE had enrichment for polycomb repressive complex SUZ12 and EZH2 signatures from actual Fib samples (Figure 6D), implicating upregulation of genes normally repressed in Fibs.

For the downregulated signatures (Figure 6D), the odd ratios showed the strongest enrichment of SUZ12 and EZH2 on the Fib sample with no significant difference in iRPENC.HQ and iPSC.RPE, suggesting that important inhibitory regulation for Fib, in real Fib samples, was reprogrammed similarly in iRPENC.HQ to reflect iPSC.RPE. Notably, iRPENC.other had weaker traces closer to Fib, following the trend that those cells destabilized and returned some fibroblastic identity. Indeed, the combined difference of the upregulated and downregulated odd ratios' analyses was more inclusive and provided greater contrast that iRPENC.HQ were reprogrammed close to iPSC.RPE.

Taken together, cell signature analysis with *in silico* regulon detection and experimental ChIP-seq signatures could each relate the reprogramming trends and distinguish unique aspects about our iRPE system's unprecedented loss of donor cell identity and the important small-molecule treatments.

iRPENC integrated to host retina *in vivo*

iRPENC cells of the same origin were used for scRNA-seq and albino rat subretinal transplant (Figure 3F). Notably, 6 weeks post-transplant, the iRPENC added pigmentation to the albino retinas that increased for approximately 5 months and was imaged during dissection for cryosection and immunohistochemistry (IHC) (Figure 7A). H&E stains showed pigmented cobblestone cells in many areas, particularly interfacing with host photoreceptor outer segments (Figure 7A). A proximal cryosection of the same transplanted area stained with EGFP antibody in the RPE layer detailing cobblestone morphology (Figure S7A). Transplanted iRPENC cells were sometimes atop host albino RPEs, with notably similar morphology and H&E stain characteristics. In some cases, RPE-like cells with weak pigment speckles were noted atop the retina ganglion cell layer, which can happen when transplants leak cells to the vitreous. Curiously, some pigment, or pigmented cells, appeared at the outer nuclear layer *membrana limitans externa*, which piqued interest for material transfer or mislocalization between the pigmented iRPENC and host cells (Figure 7A).

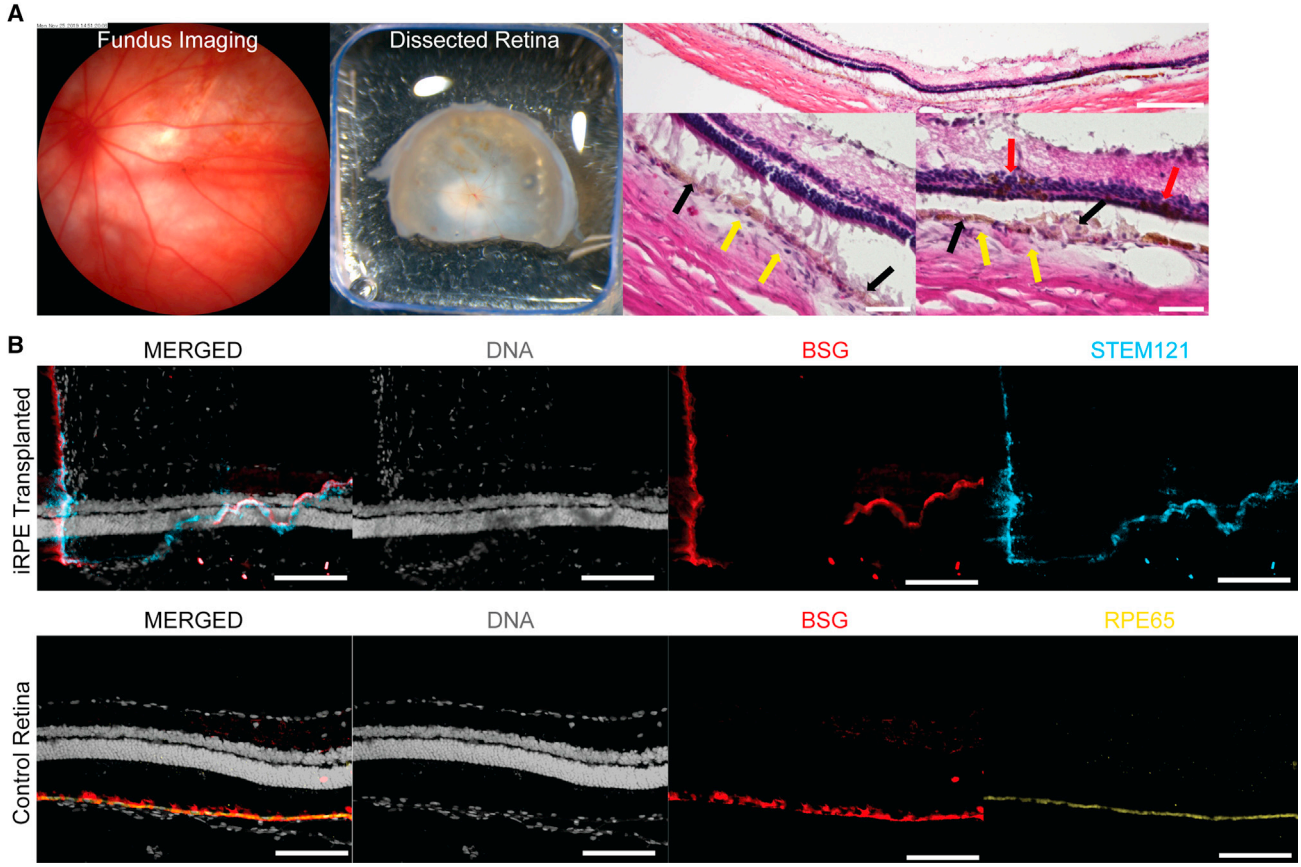

Figure 7. iRPE system cells validation *in vivo*

(A) Live fundus imaging of iRPENC transplanted albino rat retina (left) with apparent pigmentation during dissection (mid). Cryosection H&E stains (right, low mag (upper) high mag (lower x2)) show pigmented RPE-like cells (black arrows) in expected areas sometimes interfacing photoreceptor outer segments. Note: A non-pigmented RPE layer is indicated (yellow arrows), and out-of-place pigmentation is also noted (red arrows). Upper scale bar = 200 μm, lower scale bars = 50 μm.

(B) A proximal cryosection (upper) to (A) H&E stains was used for IHC against BSG (red) and human cytosol-specific STEM121 (light blue), with DNA counterstain (light gray). An untreated control retina (lower) was used for comparable IHC methods with BSG (red) and RPE65 (yellow) and DNA counterstain (light gray). Scale bars = 100 μm. Note: The iRPE transplanted retina tissue was loosened by HIER and dislocated.

To validate iRPENC positioning and polarity, we prepared IHC of intervening cryosections proximal to the H&E-stained sections in Figure 7A. To label transplanted iRPENC cells, we used heat-induced epitope retrieval (HIER) to specifically label human cell cytosol with STEM121 antibody (Tu et al., 2019). HIER consistently caused the STEM121+ iRPENC/RPE cell and choroid to detach from the neural retinal layers and "flop" to the side, suggesting that the iRPENC interface with rat photoreceptors was not so strong (Figure 7B). We found that the apical RPE marker BSG (Deora et al., 2004) had labeled the apical face of the RPE cell layer opposite the basal choroid, and, expectedly, many STEM121+ cells colocalized with the apical BSG (Figure 7B). To validate BSG detection in host RPE cells and our HIER IHC methods, we performed BSG and RPE65 HIER IHC on control retina cryosections, and the complete retinal lamina remained intact (Figure 7B).

Taken together, these observations strengthen the notion that optimized iRPE reprogramming system conditions reprogram human somatic cells into stabilized cells with subjective and objective metrics for RPE identity that could mature, integrate, and interface in transplanted host retinas for a significant time.

DISCUSSION

Cell reprogramming

Our relatively quick iRPE system generates cells resembling human RPE characterized by form, function, and gene

regulation. Importantly, our iRPE cells hold the hallmark of stability after conditional reprogramming is stopped; a state not achieved by previous iRPE systems (D'Alessio et al., 2015; Rackham et al., 2016; Zhang et al., 2014). We recognize the importance of previous reports variably employing *MITF*, *OTX2*, and *CRX* to induce RPE-like features (D'Alessio et al., 2015; Zhang et al., 2014). Still, prior iRPE reports ostensibly claimed "direct reprogramming," while relying on pluripotency inducing factors *OTX2* (Buecker et al., 2014; Thomson and Yu, 2012) and *KLF4* (Zhang et al., 2014). Important to the cell reprogramming field, "direct reprogramming" may be a misnomer, since most reprogramming system cells change across diverse states over significant time. For consideration, we wonder how any slow/non-dividing somatic state could readily become a distant somatic state effectively without precursor programs that often predicate survival and generative identity. This study exploits that wonder to coordinate TFs for plasticity, precursor, lineage, and end-state. Given that MET was evident in the first week, and cell death/survival was obvious, we anticipate that tumor suppressors such as p53 or Rb may perturb iRPE reprogramming or select critical cell states and genomic stability (Kareta et al., 2015; Marión et al., 2009; Samavarchi-Tehrani et al., 2010).

Among the TFs in this iRPE system, microphthalmia-associated TF (*MITF*) is a regulator of RPE differentiation (Adijanto et al., 2012; Hansson et al., 2015) that critically cooperates with Orthodenticle homeobox 2 (*OTX2*) for RPE development (Bharti et al., 2006, 2012; Ramón Martínez-Morales et al., 2004). Both *MITF* and *OTX2* are pioneering TFs (Soufi et al., 2015), and *OTX2* is developmentally retained from primed pluripotency as an organizer/specifier/reprogrammer (Buecker et al., 2014; Shahbazi et al., 2017; Thomson and Yu, 2012), through the neural plate, optic vesicle, and RPE specification (Hever et al., 2006). *LIN28* and *MYCL*, the "hUL" cassette for iPSC reprogramming enhancement (Okita et al., 2011), are also involved in retinal regenerating reprogramming (Luz-Madrigal et al., 2014). LIN28 binds and neutralizes *Let-7*, a promiscuous and broadly expressed miRNA somatic cell identity "lock" against plasticity, reprogramming, and state change. *MYCL* is a form of *MYC*, which cooperates with reprogramming TFs by holding open newly pioneered nucleosome-bound genomic DNA (Soufi et al., 2015). The combination (*MITF*, *OTX2*, *LIN28*, *MYCL*) was improved by *CRX*, a powerful Orthodenticle homeobox TF involved in various aspects of retinal differentiation and early RPE fate (Esumi et al., 2009; Furukawa et al., 1997).

CRX was important to this iRPE system and was identified by SCENIC as a distinguishing regulon for iPSC.RPE and iRPENC.HQ cells. However, *CRX* is lowly expressed or turned off *in vivo* as RPE matures, highlighting a potential role in regenerative medicine. Comparable MITF and CRX regulons in iPSC.RPE and iRPENC.HQ, among OTX2 regulon lacking cells, provide a strong backdrop for interpreting necessary transient, or lasting, reprogramming TFs; indeed, most iRPENCs did not have detectable endogenous *OTX2*. Weak iRPENC.HQ signatures for PAX6_extended and SOX9 regulons suggest value for other TFs that could not be used from day 0 in our iRPE system. Exploring different timing or other TF candidates may improve iRPENCs. The fact that exogenous PAX6 was required in all prior iRPE systems, yet was toxic in ours, indicates that our iRPE system genomic reprogramming mechanisms may be very different and perhaps responsible for its gains. Importantly, the iRPENC.HQ stability is likely due to the loss of Fib-specific regulon activity. Perhaps effective reprogramming was achieved, leaving a fraction of donor cell gene regulatory networks to address, and only if they affect the safety or function of the target autologous RPE cell product.

Cell identity

iRPENC had characteristics of RPE *in vitro* and *in vivo*. iRPENCs survived, expressed a maturation reporter, pigmented, and integrated into host RPE layers, sometimes interfacing with host photoreceptors. The scRNA-seq analysis revealed distinct "high-quality" iRPE cells that stabilized toward RPE cell identity and whose generation was improved by NIC and CTM treatment. Both RF and RNA velocity approaches objectively strengthened the subjective interpretations and further identified cells with high RPE gene expression and regulation. Taken together, the bioinformatics tools helped to characterize and understand the iRPE system and important cell identities among extensive data we will continue to explore.

Bulking up

In basic research, we can explore nature willy nilly, yet medicine is bound by economies of scale and practical finance. The adage "time is money" holds true in medicine, inspiring research for shortcuts toward autologous or compatible cell therapies. In that context, individual iRPE colonies were irrelevant, and only bulk cultures had robust cell number expansion toward the necessary excess from which biomedical products are purified. Surprisingly, NIC and CTM provided an unforeseen role in iRPE cell identity and selection, although co-development of the iRPE reprogramming system with plausible cell purification technologies may be necessary (Miki et al., 2015; Ota et al., 2018; Plaza Reyes et al., 2020). We roughly start with 125k cells and observe ~125 colonies, demonstrating a crude efficiency of 1:1,000 cells and not outstanding from other reprogramming systems. Ultimately, tens of millions of iRPE-like cells are generated in bulk, and data

in this study provide many leads for practical high-quality stable RPE-like purification.

EXPERIMENTAL PROCEDURES

Human Fib culture

BJ human foreskin Fibs (ATCC) and human dermal Fibs (ATCC) were cultured in Fib culture media (FCM) that consisted of 90% DMEM-high glucose, 10% tetracycline-free fetal bovine serum (FBS), and 1% penicillin streptomycin (P/S) with standard protocols on gelatin-coated culture plates. Cells were passaged at ~85%–90% confluent for expansion or to initiate reprogramming experiments.

iRPE reprogramming

iRPE media consisted of 85% DMEM/F12 + GlutaMax (1X), 15% knockout serum replacement, 1% MEM non-essential amino acids, 1% N-2 supplement (all filtered via a 0.22 μm polyethersulfone (PES)) prepared as frozen aliquots. One percent P/S is added fresh, and in the first 10 days of reprogramming, basic Fib growth factor (bFGF) is added to a final concentration of at 10 ng/mL with 2-mercaptoethanol (2ME) at 1:1,000 dilution. Doxycycline is added at 1 μg/mL (see Figure 1) for the phase 1 media. Phase 2 media consisted of all the above-mentioned reagents except for bFGF and 2ME.

Generally, a 10-cm plate coated with 0.1% gelatin and plated with 650,000 Fibs with conditional doxycycline-inducible reprogramming sets were designated as "programs" (e.g., program 2, set 2 = P2.2). Fibs ready to reprogram were reprogrammed in 6-W plates. Briefly, target wells of 6-W plates were coated with 1.5 mL of 1:150 iMatrix511/CMF-DPBS substrate for 1 h at room temperature. Fibs were passaged to yield ~125,000 cells/1.5 mL FCM per well and then incubated at 37°C 16–24 h before reprogramming medium (phase 1 iRPE medium) was added. Fibs were later checked to ensure that the cells plated as single evenly dispersed cells. The addition of the reprogramming medium marks the beginning of reprogramming as day 0. The phase 1 medium was added fresh at 2 mL every day for a total of 10 continuous days. On day 10, the phase 1 medium was replaced with phase 2 medium (no bFGF or 2ME) at 2 mL every other day.

Phase 2 media was used until ~ days 28–32, when the cells were passed in bulk to an iMatrix511 coated 6-W plate. Cell passage was as described with Fibs but with phase 2 medium containing 10% FBS to neutralize trypsin prior to spin-down. In some cases, defined trypsin inhibitor was used. Reprogramming cells were re-plated between 300,000 and 500,000 cells/well of a 6-W plate in phase 2 medium and incubated at 37°C until for ~48 h before changing the medium. On ~ day 36 phase 2 medium was prepared with fresh NIC [5–10 mM] and CTM [40–80 nM] (NC) and fed every other day for 10–12 days. Cells that did not receive NC were fed the same medias excluding those molecules. After the last feed with NC, the reprogramming cells were fed phase 2 medium once more, before culture in maturation medium ~ day 50. Note: If necessary, colonies were counted on day 9, and the diameter of the colonies were measured on day 13.

iRPE/iPSC.RPE maturation media culture (SFRM-B27)

Maturation media contained 70% DMEM-low glucose, 30% Nutrient Mixture F-12 Ham, 1% GlutaMax (100X), 2% B-27 supplement (all filtered via a 0.22 μm PES), and stored in frozen aliquots. Fresh 1% P/S, 0.5–1 μM SB431542, and 10 ng/mL bFGF is added before use.

On ~ day 50 of iRPE reprogramming, the medium is changed to the maturation media (SFRM-B27) with 1 μg/mL doxycycline. The doxycycline concentration is gradually reduced from 1 μg/mL for the first and second feeds, and then 0.5 μg/mL for the next two feeds. From the fifth feed with maturation media, doxycycline was not added. iRPE or iPSC.RPE were fed maturation media every other day, as necessary. Note: iPSC.RPE could be fed maturation media with or without doxycycline without consequence, since they did not have doxycycline-inducible reprogramming factors.

Statistics

For Figure 2B (left and right) and Figure 3C, Microsoft Excel was used to barplot means, and the add-in Analysis ToolPak was used to perform two-sample t tests and ANOVA statistical tests.

Data and code availability

All analysis codes used in this study are available upon request. Raw and processed sequence data are accessible with accession number GEO: GSE166935.

5K Human PBMC dataset used for RF experiments is available from 10x Genomics as 5k PBMCs from a healthy donor (v. 3 chemistry).

SUPPLEMENTAL INFORMATION

Supplemental information can be found online at https://doi.org/10.1016/j.stemcr.2021.12.008.

AUTHOR CONTRIBUTIONS

Conceptualization, C.K.; methodology, C.K. and I.N.W.; cryosections, J.S., M.N., H.H., and H.S.; formal analysis, C.K. and I.N.W.; investigation, C.K., I.N.W., I.A., B.K., H.H.C., K.K., H.H., and M.M.; resources, C.K., A.T., J.S., I.A., B.K., P.C., E.A., Mi.T., Y.S., M.M., and Ma.T.; writing—original draft, C.K.; writing—revision and editing, C.K., I.N.W., A.M., P.C., I.A., and E.A.; visualization, C.K., H.S., H.H., M.N., and I.N.W.; project supervision, C.K. and Ma.T.; retina aspect supervision: M.M., A.M., and Ma.T.; bioinformatics aspect supervision: E.A., I.A., T.K., B.K., and P.C.; project administration, C.K. and Ma.T.; funding acquisition, C.K., M.M., and Ma.T.

CONFLICT OF INTERESTS

C.K., M.T., and I.N.W. have filed for patent on related technology.

ACKNOWLEDGMENTS

We honor the help and support members of the RIKEN Lab for Retinal Regeneration with special mention for Sunao Sugita. We are grateful for Grace Lidgerwood and Alice Pébay of the University of Melbourne, Australia, and Anne Senabouth and Joseph Powell of the Garvan Weizmann Center for Cellular Genomics, Australia,

for sharing their ES cell-derived RPE scRNA-seq data tables for use in our study. We greatly appreciate the help of Teruaki Kitakura of RIKEN Center for Integrative Medical Sciences (DGM), Japan, for technical support and setting the computing environment. We also thank Osamu Nishimura and the Shigehiro Kuraku Lab at RIKEN for providing an HPC for initial Cell Ranger processing.

Received: April 1, 2021
Revised: December 13, 2021
Accepted: December 14, 2021
Published: January 13, 2022

REFERENCES

Abugessaisa, I., Noguchi, S., Cardon, M., Hasegawa, A., Watanabe, K., Takahashi, M., Suzuki, H., Katayama, S., Kere, J., and Kasukawa, T. (2020). Quality assessment of single-cell RNA sequencing data by coverage skewness analysis. bioRxiv https://doi.org/10.1101/2019.12.31.890269.

Adijanto, J., Castorino, J.J., Wang, Z.-X., Maminishkis, A., Grunwald, G.B., and Philp, N.J. (2012). Microphthalmia-associated transcription factor (MITF) promotes differentiation of human retinal pigment epithelium (RPE) by regulating microRNAs-204/211 expression. J. Biol. Chem. *287*, 20491–20503.

Aibar, S., González-Blas, C.B., Moerman, T., Huynh-Thu, V.A., Imrichova, H., Hulselmans, G., Rambow, F., Marine, J.-C., Geurts, P., Aerts, J., et al. (2017). SCENIC: single-cell regulatory network inference and clustering. Nat. Methods *14*, 1083–1086.

Bharti, K., Nguyen, M.-T.T., Skuntz, S., Bertuzzi, S., and Arnheiter, H. (2006). The other pigment cell: specification and development of the pigmented epithelium of the vertebrate eye. Pigment Cell Res. *19*, 380–394.

Bharti, K., Gasper, M., Ou, J., Brucato, M., Clore-Gronenborn, K., Pickel, J., and Arnheiter, H. (2012). A regulatory loop involving PAX6, MITF, and WNT signaling controls retinal pigment epithelium development. PLoS Genet. *8*, e1002757.

Breiman, L. (2001). Random forests. Mach. Learn. *45*, 5–32.

Buecker, C., Srinivasan, R., Wu, Z., Calo, E., Acampora, D., Faial, T., Simeone, A., Tan, M., Swigut, T., and Wysocka, J. (2014). Reorganization of enhancer patterns in transition from naive to primed pluripotency. Cell Stem Cell *14*, 838–853.

Butler, A., Hoffman, P., Smibert, P., Papalexi, E., and Satija, R. (2018). Integrating single-cell transcriptomic data across different conditions, technologies, and species. Nat. Biotechnol. *36*, 411–420.

D'Alessio, A.C., Fan, Z.P., Wert, K.J., Baranov, P., Cohen, M.A., Saini, J.S., Cohick, E., Charniga, C., Dadon, D., Hannett, N.M., et al. (2015). A systematic approach to identify candidate transcription factors that control cell identity. Stem Cell Rep. *5*, 763–775.

Deora, A.A., Gravotta, D., Kreitzer, G., Hu, J., Bok, D., and Rodriguez-Boulan, E. (2004). The basolateral targeting signal of CD147 (EMMPRIN) consists of a single leucine and is not recognized by retinal pigment epithelium. Mol. Biol. Cell *15*, 4148–4165.

Esumi, N., Oshima, Y., Li, Y., Campochiaro, P.A., and Zack, D.J. (2004). Analysis of the VMD2 promoter and implication of E-box binding factors in its regulation. J. Biol. Chem. *279*, 19064–19073.

Esumi, N., Kachi, S., Hackler, L., Masuda, T., Yang, Z., Campochiaro, P.A., and Zack, D.J. (2009). BEST1 expression in the retinal pigment epithelium is modulated by OTX family members. Hum. Mol. Genet. *18*, 128–141.

Furukawa, T., Morrow, E.M., and Cepko, C.L. (1997). Crx, a novel otx-like homeobox gene, shows photoreceptor-specific expression and regulates photoreceptor differentiation. Cell *91*, 531–541.

Gal, A., Li, Y., Thompson, D.A., Weir, J., Orth, U., Jacobson, S.G., Apfelstedt-Sylla, E., and Vollrath, D. (2000). Mutations in MERTK, the human orthologue of the RCS rat retinal dystrophy gene, cause retinitis pigmentosa. Nat. Genet. *26*, 270–271.

Gu, S., Thompson, D.A., Srikumari, C.R.S., Lorenz, B., Finckh, U., Nicoletti, A., Murthy, K.R., Rathmann, M., Kumaramanickavel, G., Denton, M.J., et al. (1997). Mutations in RPE65 cause autosomal recessive childhood–onset severe retinal dystrophy. Nat. Genet. *17*, 194–197.

Hansson, M.L., Albert, S., Somermeyer, L.G., Peco, R., Mejía-Ramírez, E., Montserrat, N., and Belmonte, J.C.I. (2015). Efficient delivery and functional expression of transfected modified mRNA in human embryonic stem cell-derived retinal pigmented epithelial cells. J. Biol. Chem. *290*, 5661–5672.

Haruta, M., Sasai, Y., Kawasaki, H., Amemiya, K., Ooto, S., Kitada, M., Suemori, H., Nakatsuji, N., Ide, C., Honda, Y., et al. (2004). In vitro and in vivo characterization of pigment epithelial cells differentiated from primate embryonic stem cells. Investig. Opthalmol. Vis. Sci. *45*, 1020.

Hever, A.M., Williamson, K.A., and Heyningen, V.V. (2006). Developmental malformations of the eye: the role of PAX6, SOX2 and OTX2. Clin. Genet. *69*, 459–470.

Iwafuchi-Doi, M., and Zaret, K.S. (2014). Pioneer transcription factors in cell reprogramming. Genes Dev. *28*, 2679–2692.

Iwasaki, Y., Sugita, S., Mandai, M., Yonemura, S., Onishi, A., Ito, S., Mochizuki, M., Ohno-Matsui, K., and Takahashi, M. (2016). Differentiation/purification protocol for retinal pigment epithelium from mouse induced pluripotent stem cells as a research tool. PLoS One *11*, e0158282.

Kamao, H., Mandai, M., Okamoto, S., Sakai, N., Suga, A., Sugita, S., Kiryu, J., and Takahashi, M. (2014). Characterization of human induced pluripotent stem cell-derived retinal pigment epithelium cell sheets aiming for clinical application. Stem Cell Rep. *2*, 205–218.

Kareta, M.S., Gorges, L.L., Hafeez, S., Benayoun, B.A., Marro, S., Zmoos, A.-F., Cecchini, M.J., Spacek, D., Batista, L.F.Z., O'Brien, M., et al. (2015). Inhibition of pluripotency networks by the Rb tumor suppressor restricts reprogramming and tumorigenesis. Cell Stem Cell *16*, 39–50.

Klein, R., Klein, B.E.K., and Linton, K.L.P. (1992). Prevalence of age-related maculopathy: the beaver dam eye study. Ophthalmology *99*, 933–943.

Kuroda, T., Yasuda, S., Kusakawa, S., Hirata, N., Kanda, Y., Suzuki, K., Takahashi, M., Nishikawa, S.-I., Kawamata, S., and Sato, Y. (2012). Highly sensitive in vitro methods for detection of residual undifferentiated cells in retinal pigment epithelial cells derived from human iPS cells. PLoS One *7*, e37342.

La Manno, G., Soldatov, R., Zeisel, A., Braun, E., Hochgerner, H., Petukhov, V., Lidschreiber, K., Kastriti, M.E., Lönnerberg, P., Furlan, A., et al. (2018). RNA velocity of single cells. Nature *560*, 494–498.

Li, R., Liang, J., Ni, S., Zhou, T., Qing, X., Li, H., He, W., Chen, J., Li, F., Zhuang, Q., et al. (2010). A mesenchymal-to-epithelial transition initiates and is required for the nuclear reprogramming of mouse fibroblasts. Cell Stem Cell *7*, 51–63.

Liao, J.-L., Yu, J., Huang, K., Hu, J., Diemer, T., Ma, Z., Dvash, T., Yang, X.-J., Travis, G.H., Williams, D.S., et al. (2010). Molecular signature of primary retinal pigment epithelium and stem-cell-derived RPE cells. Hum. Mol. Genet. *19*, 4229–4238.

Lidgerwood, G.E., Senabouth, A., Smith-Anttila, C.J.A., Gnanasambandapillai, V., Kaczorowski, D.C., Amann-Zalcenstein, D., Fletcher, E.L., Naik, S.H., Hewitt, A.W., Powell, J.E., et al. (2020). Transcriptomic profiling of human pluripotent stem cell-derived retinal pigment epithelium over time. Genomics Proteomics Bioinformatics *19*, 223–242.

Luecken, M.D., and Theis, F.J. (2019). Current best practices in single-cell RNA-seq analysis: a tutorial. Mol. Syst. Biol. *15*, e8746.

Luz-Madrigal, A., Grajales-Esquivel, E., McCorkle, A., DiLorenzo, A.M., Barbosa-Sabanero, K., Tsonis, P.A., and Del Rio-Tsonis, K. (2014). Reprogramming of the chick retinal pigmented epithelium after retinal injury. BMC Biol. *12*, 28.

Maeda, T., Lee, M.J., Palczewska, G., Marsili, S., Tesar, P.J., Palczewski, K., Takahashi, M., and Maeda, A. (2013). Retinal pigmented epithelial cells obtained from human induced pluripotent stem cells possess functional visual cycle enzymes in vitro and in vivo. J. Biol. Chem. *288*, 34484–34493.

Mandai, M., Watanabe, A., Kurimoto, Y., Hirami, Y., Morinaga, C., Daimon, T., Fujihara, M., Akimaru, H., Sakai, N., Shibata, Y., et al. (2017). Autologous induced stem-cell–derived retinal cells for macular degeneration. N. Engl. J. Med. *376*, 1038–1046.

Marión, R.M., Strati, K., Li, H., Murga, M., Blanco, R., Ortega, S., Fernandez-Capetillo, O., Serrano, M., and Blasco, M.A. (2009). A p53-mediated DNA damage response limits reprogramming to ensure iPS cell genomic integrity. Nature *460*, 1149–1153.

Maruotti, J., Sripathi, S.R., Bharti, K., Fuller, J., Wahlin, K.J., Ranganathan, V., Sluch, V.M., Berlinicke, C.A., Davis, J., Kim, C., et al. (2015). Small-molecule–directed, efficient generation of retinal pigment epithelium from human pluripotent stem cells. Proc. Natl. Acad. Sci. U S A *112*, 10950–10955.

Masuda, T., and Esumi, N. (2010). SOX9, through interaction with microphthalmia-associated transcription factor (MITF) and OTX2, regulates *BEST1* expression in the retinal pigment epithelium. J. Biol. Chem. *285*, 26933–26944.

McInnes, L., Healy, J., and Melville, J. (2018). UMAP: uniform manifold approximation and projection for dimension reduction. arXiv, 1802.03426 Cs Stat.

Miki, K., Endo, K., Takahashi, S., Funakoshi, S., Takei, I., Katayama, S., Toyoda, T., Kotaka, M., Takaki, T., Umeda, M., et al. (2015). Efficient detection and purification of cell populations using synthetic MicroRNA switches. Cell Stem Cell *16*, 699–711.

Najm, F.J., Lager, A.M., Zaremba, A., Wyatt, K., Caprariello, A.V., Factor, D.C., Karl, R.T., Maeda, T., Miller, R.H., and Tesar, P.J. (2013). Transcription factor–mediated reprogramming of fibroblasts to expandable, myelinogenic oligodendrocyte progenitor cells. Nat. Biotechnol. *31*, 426–433.

Okita, K., Matsumura, Y., Sato, Y., Okada, A., Morizane, A., Okamoto, S., Hong, H., Nakagawa, M., Tanabe, K., Tezuka, K., et al. (2011). A more efficient method to generate integration-free human iPS cells. Nat. Methods *8*, 409–412.

Ota, S., Horisaki, R., Kawamura, Y., Ugawa, M., Sato, I., Hashimoto, K., Kamesawa, R., Setoyama, K., Yamaguchi, S., Fujiu, K., et al. (2018). Ghost cytometry. Science *360*, 1246–1251.

Pang, Z.P., Yang, N., Vierbuchen, T., Ostermeier, A., Fuentes, D.R., Yang, T.Q., Citri, A., Sebastiano, V., Marro, S., Südhof, T.C., et al. (2011). Induction of human neuronal cells by defined transcription factors. Nature *476*, 220–223.

Petrukhin, K., Koisti, M.J., Bakall, B., Li, W., Xie, G., Marknell, T., Sandgren, O., Forsman, K., Holmgren, G., Andreasson, S., et al. (1998). Identification of the gene responsible for best macular dystrophy. Nat. Genet. *19*, 241–247.

Petukhov, V., Guo, J., Baryawno, N., Severe, N., Scadden, D.T., Samsonova, M.G., and Kharchenko, P.V. (2018). dropEst: pipeline for accurate estimation of molecular counts in droplet-based single-cell RNA-seq experiments. Genome Biol. *19*, 78.

Plaza Reyes, A., Petrus-Reurer, S., Padrell Sánchez, S., Kumar, P., Douagi, I., Bartuma, H., Aronsson, M., Westman, S., Lardner, E., André, H., et al. (2020). Identification of cell surface markers and establishment of monolayer differentiation to retinal pigment epithelial cells. Nat. Commun. *11*, 1609.

Rackham, O.J.L., Firas, J., Fang, H., Oates, M.E., Holmes, M.L., Knaupp, A.S., Suzuki, H., Nefzger, C.M., Daub, C.O., Shin, J.W., et al. (2016). A predictive computational framework for direct reprogramming between human cell types. Nat. Genet. *48*, 331–335.

Ramón Martínez-Morales, J., Rodrigo, I., and Bovolenta, P. (2004). Eye development: a view from the retina pigmented epithelium. Bioessays *26*, 766–777.

Samavarchi-Tehrani, P., Golipour, A., David, L., Sung, H.-K., Beyer, T.A., Datti, A., Woltjen, K., Nagy, A., and Wrana, J.L. (2010). Functional genomics reveals a BMP-driven mesenchymal-to-epithelial transition in the initiation of somatic cell reprogramming. Cell Stem Cell *7*, 64–77.

Shahbazi, M.N., Scialdone, A., Skorupska, N., Weberling, A., Recher, G., Zhu, M., Jedrusik, A., Devito, L.G., Noli, L., Macaulay, I.C., et al. (2017). Pluripotent state transitions coordinate morphogenesis in mouse and human embryos. Nature *552*, 239–243.

Smith, W., Assink, J., Klein, R., Mitchell, P., Klaver, C.C.W., Klein, B.E.K., Hofman, A., Jensen, S., Wang, J.J., and Jong, P.T.D. (2001). Risk factors for age-related macular degeneration: pooled findings from three continents. Ophthalmology *108*, 697–704.

Soufi, A., and Zaret, K. (2013). Understanding impediments to cellular conversion to pluripotency by assessing the earliest events in ectopic transcription factor binding to the genome. Cell Cycle *12*, 1487–1491.

Soufi, A., Donahue, G., and Zaret, K.S. (2012). Facilitators and impediments of the pluripotency reprogramming factors' initial engagement with the genome. Cell *151*, 994–1004.

Soufi, A., Garcia, M.F., Jaroszewicz, A., Osman, N., Pellegrini, M., and Zaret, K.S. (2015). Pioneer transcription factors target partial

DNA motifs on nucleosomes to initiate reprogramming. Cell *161*, 555–568.

Stuart, T., Butler, A., Hoffman, P., Hafemeister, C., Papalexi, E., Mauck, W.M., Hao, Y., Stoeckius, M., Smibert, P., and Satija, R. (2019). Comprehensive integration of single-cell data. Cell *177*, 1888–1902.e21.

Takahashi, K., Tanabe, K., Ohnuki, M., Narita, M., Ichisaka, T., Tomoda, K., and Yamanaka, S. (2007). Induction of pluripotent stem cells from adult human fibroblasts by defined factors. Cell *131*, 861–872.

Thomson J.A., and Yu J. (2012). Composition comprising recombinant nucleic acid encoding Sox2, Oct-4, Nanog and Lin28 (US Patent No. 8,183,038).

Tomaru, Y., Hasegawa, R., Suzuki, T., Sato, T., Kubosaki, A., Suzuki, M., Kawaji, H., Forrest, A.R.R., Hayashizaki, Y., Shin, J.W., et al. (2014). A transient disruption of fibroblastic transcriptional regulatory network facilitates trans-differentiation. Nucleic Acids Res. *42*, 8905–8913.

Trapnell, C., Cacchiarelli, D., Grimsby, J., Pokharel, P., Li, S., Morse, M., Lennon, N.J., Livak, K.J., Mikkelsen, T.S., and Rinn, J.L. (2014). The dynamics and regulators of cell fate decisions are revealed by pseudotemporal ordering of single cells. Nat. Biotechnol. *32*, 381–386.

Tu, H.-Y., Watanabe, T., Shirai, H., Yamasaki, S., Kinoshita, M., Matsushita, K., Hashiguchi, T., Onoe, H., Matsuyama, T., Kuwahara, A., et al. (2019). Medium- to long-term survival and functional examination of human iPSC-derived retinas in rat and primate models of retinal degeneration. EBioMedicine *39*, 562–574.

Verbakel, S.K., van Huet, R.A.C., Boon, C.J.F., den Hollander, A.I., Collin, R.W.J., Klaver, C.C.W., Hoyng, C.B., Roepman, R., and Klevering, B.J. (2018). Non-syndromic retinitis pigmentosa. Prog. Retin. Eye Res. *66*, 157–186.

Williams, L.A., Davis-Dusenbery, B.N., and Eggan, K.C. (2012). SnapShot: directed differentiation of pluripotent stem cells. Cell *149*, 1174–1174.e1.

Zhang, K., Liu, G.-H., Yi, F., Montserrat, N., Hishida, T., Esteban, C.R., and Belmonte, J.C.I. (2014). Direct conversion of human fibroblasts into retinal pigment epithelium-like cells by defined factors. Protein Cell *5*, 48–58.

Zhao, Y., Zhao, T., Guan, J., Zhang, X., Fu, Y., Ye, J., Zhu, J., Meng, G., Ge, J., Yang, S., et al. (2015). A XEN-like state bridges somatic cells to pluripotency during chemical reprogramming. Cell *163*, 1678–1691.